Magic wavelengths for $6s_{1/2} \rightarrow 5d_{3/2,5/2}$ transitions of Yb^+ ions

Ting Chen(陈婷)[1,†], Lei Wu(吴磊)[1,†], Ru-Kui Zhang(张儒奎)[1], Yong-Bo Tang(唐永波)[2], Jun Jiang(蒋军)[1,‡], and Chen-Zhong Dong(董晨钟)[1]

[1] *Key Laboratory of Atomic and Molecular Physics and Functional Materials of Gansu Province, College of Physics and Electronic Engineering, Northwest Normal University, Lanzhou* 730070, *China*
[2] *Physics Teaching and Experiment Center, Shenzhen Technology University, Shenzhen* 518118, *China*

(Received 4 November 2022; revised manuscript received 12 January 2023; accepted manuscript online 16 February 2023)

The wave functions, energy levels and matrix elements of Yb^+ ions are calculated using the relativistic configuration interaction plus core polarization (RCICP) method. The static and dynamic electric dipole polarizabilities of the ground state and low-lying excited states are determined. Then, the magic wavelengths of the magnetic sublevel $6s_{1/2,m=1/2} \rightarrow 5d_{3/2,m=\pm3/2,\pm1/2}$ and $6s_{1/2,m=1/2} \rightarrow 5d_{5/2,m=\pm5/2,\pm3/2,\pm1/2}$ transitions in the linearly, right-handed, and left-handed polarized light are further determined. The dependence of the magic wavelengths upon the angle between the direction of magnetic field and the direction of laser polarization is analyzed.

Keywords: matrix elements, polarizabilities, magic wavelengths, relativistic configuration interaction plus core polarization (RCICP) method

PACS: 31.15.ap, 32.10.Dk **DOI:** 10.1088/1674-1056/acbc6c

1. Introduction

The interaction between the laser field and the atoms can cause ac Stark shift, which is one of the most important factors that influence the atomic transition frequency. In order to reduce the impact of the ac Stark shift, magic-wavelength trapping was introduced in Refs. [1,2], in which the shifts of a given pair of energy levels are the same as each other. The magic-wavelength trapping has been extensively used in optical lattice clocks,[3–5] and the performance and accuracy of optical lattice clocks have been greatly improved.[6,7]

Yb^+ is one of the good candidates for ultrahigh-precision optical clocks.[8,9] Yb^+ optical clocks have been studied as promising optical frequency standards by the groups of National Physical Laboratory in the UK[10] and German Institute of Physikalisch-Technische Bundesanstalt.[11–13] The $[4f^{14}5d]\ ^2D_{3/2}$ and $[4f^{14}5d]\ ^2D_{5/2}$ states of Yb^+ ions are long-lived metastable states with lifetimes of about 52.7(2.4) ms[14] and 7.2(3) ms,[15] respectively. The $6s_{1/2} \rightarrow 5d_{3/2}$ transition wavelength lies in the optical range with a natural linewidth of about 3.1 Hz.[16] Consequently, the quality factor Q, the ratio of transition frequency to natural linewidth, of this line is about 2.2×10^{14}.[17] In addition, Yb^+ ions can also be used for probing parity nonconservation effect,[18] exploring fundamental physics,[19,20] testing local Lorentz invariance,[21] and processing quantum information.[22] Due to the non-spherical symmetry structure of the $5d_{3/2,5/2}$ states, the laser polarization and direction have great influence on the magic wavelength. It is very difficult to accurately measure magic wavelengths in experiments. Additionally, for Yb^+ ions, there are a large number of electrons and it is complex to accurately calculate atomic structure parameters.[23]

In this paper, the energy levels, electric dipole (E1) matrix elements of Yb^+ ions are calculated using a semiempirical method — the so-called relativistic configuration interaction plus core polarization (RCICP) method. The electric dipole polarizabilities of the ground state $6s_{1/2}$ and low-lying excited states $6p_{1/2,3/2}$ and $5d_{3/2,5/2}$ are determined. The magic wavelengths of the $6s_{1/2} \rightarrow 5d_{3/2,5/2}$ transitions in the linearly, right-handed polarized light, and left-handed polarized light are further determined. Then, the dependence of the magic wavelengths upon the angle between the direction of magnetic field and the direction of laser polarization is analyzed. Atomic units ($m_e = 1$, $e = 1$, $\hbar = 1$) are used throughout the paper unless stated otherwise. The speed of light is chosen to be $c = 137.0359991$ in our calculations.

2. Theoretical method

A detailed description of the RCICP method has been given in Ref. [24], here we just present a brief introduction (Yb^+ ions can be considered as a single electron system, so there is no configuration interaction). The key strategy of the method is to partition a Yb^+ ion into a Yb^{2+} core plus a valence electron. The first step involves a Dirac–Fock (DF) calculation on the core of Yb^+ ions. The single-particle orbitals are written as a linear combination of the S-spinors,[25,26] which can be regarded as a relativistic generalization of the

†These authors contributed equally to this paper.
‡Corresponding author. E-mail: phyjiang@yeah.net

© 2023 Chinese Physical Society and IOP Publishing Ltd

Slater-type orbitals.

The effective Hamiltonian of the valence electron is written as

$$H = c\boldsymbol{\alpha}\cdot\boldsymbol{p} + (\boldsymbol{\beta}-1)c^2 + V_{\rm core}(\boldsymbol{r}), \tag{1}$$

where $\boldsymbol{\alpha}$ and $\boldsymbol{\beta}$ are 4×4 Dirac matrices, $\boldsymbol{p}$ is the momentum operator, c is the speed of light, and $\boldsymbol{r}$ is the position vector of the valence electron. Moreover, $V_{\rm core}(\boldsymbol{r})$ is given by

$$V_{\rm core}(\boldsymbol{r}) = -\frac{Z}{r} + V_{\rm dir}(\boldsymbol{r}) + V_{\rm exc}(\boldsymbol{r}) + V_{\rm p}(\boldsymbol{r}). \tag{2}$$

Here, Z is atomic number, r is the distance of the valence electron with respect to the origin of the coordinates. $V_{\rm dir}(\boldsymbol{r})$ and $V_{\rm exc}(\boldsymbol{r})$ denote the direct and exchange interactions of the valence electron with the core electrons, respectively.[24] The l and j-dependent polarization potential $V_{\rm p}(r)$ can be written as

$$V_{\rm p}(\boldsymbol{r}) = -\sum_{k=1}^{1}\frac{\alpha^k_{\rm core}}{2r^{2(k+1)}}\sum_{l,j} g^2_{k,l,j}(r)\,|lj\rangle\langle lj|, \tag{3}$$

where l and j are orbital and total angular momenta, respectively. $\alpha^k_{\rm core}$ is the k-th-order static polarizabilities of the core electrons ($\alpha^1_{\rm core} = 7.72$ a.u. for Yb^{2+} ions[27]), and $g^2_{k,l,j}(r) = 1-\exp[-r^{2(k+2)}/\rho^{2(k+2)}_{l,j}]$. The cutoff parameters $\rho_{l,j}$ are tuned to reproduce the binding energies of the ground state and some low-lying excited states, and the adopted parameters are listed in Table 1. The effective Hamiltonian of the valence electron is diagonalized within a large S-spinor and L-spinor basis.[26] L-spinors can be regarded as a relativistic generalization of the Laguerre-type orbitals.

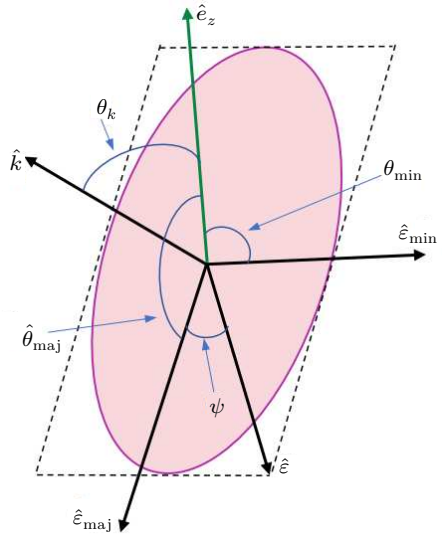


Fig. 1. Representation of the electromagnetic plane-wave geometrical parameters. The surface represents the ellipse swept out by the electric field vector in one period. The unit vector $\hat{\varepsilon}_{\rm maj}$ ($\hat{\varepsilon}_{\rm min}$) aligns with the semimajor (-minor) axis of the ellipse. $\hat{e}_z$ is the direction of magnetic field (quantization axis), which selects the direction of the magnetic field in experiment. $\hat{k}$ represents the direction of the wave vector. θ_k is the angle between $\hat{e}_z$ and $\hat{k}$. The parameters $\hat{\varepsilon}_{\rm maj}$, $\hat{\varepsilon}_{\rm min}$, and $\hat{k}$ are mutually orthogonal. $\theta_{\rm maj}$ ($\theta_{\rm min}$) is the angle between $\hat{\varepsilon}_{\rm maj}$ ($\hat{\varepsilon}_{\rm min}$) and $\hat{e}_z$. ψ is directly related to the degree of circular polarization.

Table 1. The cutoff parameters $\rho_{l,j}$ of the polarization potential of Yb^+ ions.

l	J	$\rho_{l,j}$
s	1/2	2.4687
p	1/2	2.1196
	3/2	1.9624
d	3/2	2.1842
	5/2	2.1951
f	5/2	2.2400
	7/2	1.7080

For an arbitrarily polarized light, the dynamic polarizability for an atomic state i is given by[28,29]

$$\begin{aligned}\alpha_i(\omega) &= \alpha_i^{\rm S}(\omega) + \mathcal{A}\cos\theta_k\frac{m_{j_i}}{2j_i}\alpha_i^{\rm V}(\omega)\\ &+\frac{3\cos^2\theta_{\rm p}-1}{2}\frac{3m^2_{j_i}-j_i(j_i+1)}{j_i(2j_i-1)}\alpha_i^{\rm T}(\omega),\end{aligned} \tag{4}$$

where m_{j_i} is the component of the total angular momentum j_i. It is noted that there is no tensor polarizability for the states with $j\le 1/2$. θ_k is the angle between the wave vector $\hat{k}$ and the direction of magnetic field (quantization axis $\hat{e}_z$) as defined below, $\cos\theta_k = \hat{k}\cdot\hat{e}_z$. The $\theta_{\rm p}$ relates to direction of laser polarization (polarization vector $\hat{\varepsilon}$) and $\hat{e}_z$ axis. The relevant diagram is shown in Fig. 1. For a more general geometrical interpretation of $\theta_{\rm p}$, it is useful to further introduce the parameters $\theta_{\rm maj}$, $\theta_{\rm min}$, and ψ. $\cos^2\theta_{\rm p}$ can be written in the form[30]

$$\cos^2\theta_{\rm p} = \cos^2\psi\cos^2\theta_{\rm maj} + \sin^2\psi\cos^2\theta_{\rm min}, \tag{5}$$

where the parameter $\theta_{\rm maj}$ ($\theta_{\rm min}$) is the angle between the major (minor) axis of the ellipse and the $\hat{e}_z$ axis. From the geometrical consideration, θ_k and $\theta_{\rm p}$ satisfy the relation $\cos^2\theta_k + \cos^2\theta_{\rm p}\le 1$.[28,29] The angle ψ is directly related to the degree of polarization of light. $\mathcal{A}$ represents the degree of polarization ($\mathcal{A}=0$ is linearly polarized light, $\mathcal{A}=+1$ is the right-handed, and $\mathcal{A}=-1$ is the left-handed circularly polarized light). $\alpha_i^{\rm S}(\omega)$, $\alpha_i^{\rm V}(\omega)$, and $\alpha_i^{\rm T}(\omega)$ represent the scalar, vector, and tensor polarizabilities for the state i, respectively. It can be given by

$$\alpha_i^{\rm S}(\omega) = \sum_n \frac{f_{i,n}}{\Delta E^2_{n,i}-\omega^2}, \tag{6}$$

$$\begin{aligned}\alpha_i^{\rm V}(\omega) &= 3\sqrt{\frac{6j_i(2j_i+1)}{(j_i+1)}}\times\sum_n\begin{Bmatrix}1 & 1 & 2\\ j_i & j_i & j_n\end{Bmatrix}\\ &\times(-1)^{j_i+j_n}\times\frac{f_{i,n}}{\Delta E^2_{n,i}-\omega^2}\frac{\omega}{\Delta E_{n,i}},\end{aligned} \tag{7}$$

$$\begin{aligned}\alpha_i^{\rm T}(\omega) &= 6\sqrt{\frac{5j_i(2j_i-1)(2j_i+1)}{6(j_i+1)(2j_i+3)}}\times\sum_n\begin{Bmatrix}1 & 1 & 2\\ j_i & j_i & j_n\end{Bmatrix}\\ &\times(-1)^{j_i+j_n}\times\frac{f_{i,n}}{\Delta E^2_{n,i}-\omega^2}.\end{aligned} \tag{8}$$

Here, $\Delta E_{n,i} = E_n - E_i$ is the transition energy. The E1 absorption oscillator strength $f_{i,n}$ is defined as

$$f_{i,n} = \frac{2|\langle \gamma_n\ j_n \|\boldsymbol{D}\|\ \gamma_i j_i\rangle|^2 \Delta E_{n,i}}{3(2j_i+1)}, \tag{9}$$

where γ represents all additional angular momenta in addition to the total angular momenta j.

3. Results and discussion

3.1. Dipole transition matrix elements

Due to the introduction of the polarization potential, the E1 transition operator is given by[31–33]

$$\boldsymbol{D} = \boldsymbol{r} - \left[1 - \exp\left(-\frac{r^6}{\rho^6}\right)\right]^{1/2} \frac{\alpha^1_{\rm core}\boldsymbol{r}}{r^3}. \tag{10}$$

The cutoff parameters are not the same for the initial and final states of the transition. In order to make the correction of the transition matrix elements more reasonable, the average cutoff parameters are used for the correction of the transition matrix elements.

The cutoff parameter for the polarization corrections to transition operator was fixed at $\rho = 2.16833$ a.u., generated as $\rho = 1/8 \times (2\rho_{\rm s_{1/2}} + \rho_{\rm p_{1/2}} + \rho_{\rm p_{3/2}} + \rho_{\rm d_{3/2}} + \rho_{\rm d_{5/2}} + \rho_{\rm f_{5/2}} + \rho_{\rm f_{7/2}})$.

In Table 2, we list the presently calculated reduced matrix elements for a number of principal E1 transitions of Yb^+ ions, which are compared with some theoretical[18,23,27,34–36] and experimental[37–39] results. For the resonant $6s_{1/2} \to 6p_{1/2,3/2}$ transitions, the present RCICP results agree very well with the other theoretical results,[23] but all theoretical results are larger than the experimental results[37–39] by about 7%. For the $5d_{3/2} \to 6p_{1/2,3/2}$, $5d_{3/2} \to 5f_{5/2}$, $5d_{5/2} \to 6p_{3/2}$, $5d_{5/2} \to 5f_{7/2}$, $6p_{1/2} \to 7s_{1/2}$, $6p_{1/2} \to 6d_{3/2}$, $6p_{3/2} \to 7s_{1/2}$, and $6p_{3/2} \to 6d_{3/2,5/2}$ tranitions, the reduced matrix elements are larger than 1.0 a.u., and no experimental results can be found, except for the $5d_{3/2} \to 6p_{1/2}$ transition. The present RCICP results are in good agreement with the relativistic many-body perturbation theory (RMBPT) results,[35] and the difference is less than 4%. For the $5d_{3/2} \to 6p_{1/2}$ transition, the agreement with the measurements[37,38] is better than 3%. Moreover, for the $6s_{1/2} \to 7p_{1/2,3/2}$, $5d_{3/2} \to 7p_{1/2,3/2}$, $5d_{5/2} \to 7p_{3/2}$, and $5d_{5/2} \to 5f_{5/2}$ transitions, the reduced matrix elements are all less than 1.0 a.u., and no experimental results can be found. The present RCICP results are in good agreement with the relativistic coupled-cluster (RCC) results.[27]

Table 2. Reduced E1 matrix elements (in unit a.u.) for principal transitions of Yb^+ ions. The numbers in the parentheses are uncertainties.

Transitions	RCICP	RCC(T)[18]	SD All-order[23]	RCC[27]	DF+CP[34]	RMBPT[35]	HFR+CP[36]	Expt.
$6s_{1/2} \to 6p_{1/2}$	2.63(7)	2.72(1)	2.64		2.75	2.6829	2.39	2.471(3)[37,38]
$6s_{1/2} \to 6p_{3/2}$	3.73(9)	3.83(1)	3.71		3.84	3.7676	3.09	3.36(3)[39]
$6s_{1/2} \to 7p_{1/2}$	0.08(3)			0.08(1)	0.01	0.0686		
$6s_{1/2} \to 7p_{3/2}$	0.14(6)	0.18(2)		0.11(1)	0.20	0.1530		
$5d_{3/2} \to 6p_{1/2}$	2.88(8)	3.06(2)	2.98		6.53	2.9707	2.84	2.97[37,38]
$5d_{3/2} \to 6p_{3/2}$	1.28(3)	1.35(2)	1.32	1.31(2)	2.05	1.3068	1.17	
$5d_{3/2} \to 7p_{1/2}$	0.20(8)	0.17(2)		0.14(2)	0.03	0.0829		
$5d_{3/2} \to 7p_{3/2}$	0.014(4)			0.014(5)	0.07	0.0369		
$5d_{3/2} \to 5f_{5/2}$	2.56(7)			2.43(4)	2.56			
$5d_{5/2} \to 6p_{3/2}$	3.98(10)	4.23(3)			7.52	4.1204	3.60	
$5d_{5/2} \to 7p_{3/2}$	0.10(4)				0.18	0.0229	0.74	
$5d_{5/2} \to 5f_{5/2}$	0.73(2)				0.73			
$5d_{5/2} \to 5f_{7/2}$	3.21(8)				3.24			
$6p_{1/2} \to 7s_{1/2}$	2.19(6)				2.03	2.2338	2.11	
$6p_{1/2} \to 6d_{3/2}$	3.62(9)					3.7094		
$6p_{3/2} \to 7s_{1/2}$	3.62(9)				3.32	3.7042		
$6p_{3/2} \to 6d_{3/2}$	1.84(5)					1.8899		
$6p_{3/2} \to 6d_{5/2}$	5.38(14)					5.4787		

The uncertainties of the present transition matrix elements are estimated using the method in Refs. [40,41]. For the $6s_{1/2} \to 6p_{1/2,3/2}$, $5d_{3/2} \to 6p_{1/2,3/2}$, $5d_{3/2} \to 7p_{3/2}$, $5d_{3/2} \to 5f_{5/2}$, $5d_{5/2} \to 6p_{3/2}$, $5d_{5/2} \to 5f_{5/2,7/2}$, $6p_{1/2} \to 7s_{1/2}$, $6p_{1/2} \to 6d_{3/2}$, $6p_{3/2} \to 7s_{1/2}$, $6p_{3/2} \to 6d_{3/2,5/2}$ transitions, the uncertainty is about 2.6%. For the $6s_{1/2} \to 7p_{1/2,3/2}$, $5d_{3/2} \to 7p_{1/2}$, $5d_{5/2} \to 7p_{3/2}$ transitions, the uncertainty is relatively large. In addition, we find that when the uncertainty of static electric dipole polarizability of the core is about 10%, which can cause an uncertainty of 0.4% for the transition matrix elements.

3.2. Static dipole polarizabilities

Table 3 lists the presently calculated static dipole scalar and tensor polarizabilities for the $6s_{1/2}$, $5d_{3/2}$, $5d_{5/2}$, $6p_{1/2}$, and $6p_{3/2}$ states of Yb^+ ions, along with a comparison with some available theoretical[27,35,42] and experimental results.[43] For the ground state $6s_{1/2}$, the present RCICP re-

sult is in good agreement with the results of the RCC,[27] RMBPT,[35] and relativistic model potential plus core polarization (RMP + CP) methods[42] within the uncertainty range. The differences are no more than 3%. In addition, the result of Ref. [43] is smaller than the present RCICP result by about 28%. The main reasons are that only a few E1 transitions were included in the calculation of Ref. [43], and the core contribution was completely ignored. The present scalar polarizability is in good agreement with the RCC result[27] for the $5d_{3/2}$ state, the difference is no more than 5%, and within the uncertainty range of the result of Ref. [43]. For $5d_{5/2}$, $6p_{1/2}$, and $6p_{3/2}$ states, as far as we know, there are no other theoretical and experimental results can be found.

The uncertainties of the present transition matrix elements lead to the uncertainties of 5.2% for these polarizabilities. In addition, the contribution of the negative energy states to the polarizability is estimated about 1.92×10^{-5} a.u., which can be ignored.

Table 3. Comparison of the static dipole scalar and tensor polarizabilities (in unit a.u.) of the low-lying states $6s_{1/2}$, $6p_{1/2,3/2}$ and $5d_{3/2,5/2}$ of Yb^+ ions with available experimental and theoretical results.

Methods	$6s_{1/2}$	$5d_{3/2}$		$5d_{5/2}$		$6p_{1/2}$	$6p_{3/2}$	
	α^S	α^S	α^T	α^S	α^T	α^S	α^S	α^T
RCICP	60.1(3.1)	99.1(5.2)	−69.3(3.6)	82.1(4.3)	−66.9(3.5)	−112.5(5.9)	−49.5(2.6)	4.2(2)
RCC[27]	59.3(8)	107(3)	−75(2)					
RMBPT[35]	62.04							
RMP + CP[42]	59.32							
Ref. [43]	47(9)	90(17)						
Expt.[44]			−82.5(1.3)					

3.3. Dynamic polarizabilities

When $\hat{e}_z$ axis is chosen along the wave vector $\hat{k}$, as a consequence, $\cos\theta_k = 1$ and $\cos^2\theta_p = 0$. Equation (4) is thus simplified as

$$\alpha_i(\omega) = \alpha_i^S(\omega) + \mathcal{A}\frac{m_{j_i}}{2j_i}\alpha_i^V(\omega) - \frac{3m_{j_i}^2 - j_i(j_i+1)}{2j_i(2j_i-1)}\alpha_i^T(\omega). \tag{11}$$

Figure 2 shows the dynamic polarizabilities of the $6s_{1/2,m=1/2}$ state with $\mathcal{A} = 0$ and $\mathcal{A} = \pm 1$. It is noted that there is no tensor polarizability for the ground state $6s_{1/2}$, and only scalar polarizability for the case of $\mathcal{A} = 0$, and scalar and vector polarizabilities for the case of $\mathcal{A} = \pm 1$. According to Eq. (4), the dynamic polarizabilities of atomic states with negative m for $\mathcal{A} = -1$ are the same as those of states with positive m for $\mathcal{A} = +1$, and the dynamic polarizabilities of atomic states with positive m for $\mathcal{A} = -1$ are the same as those of states with negative m for $\mathcal{A} = +1$. As can be seen clearly, the behaviors of the dynamic polarizabilities of the $6s_{1/2,m=1/2}$ state in the $\mathcal{A} = +1$ are different from the case of $\mathcal{A} = 0$ and $\mathcal{A} = -1$, these differences are caused by the dynamic vector polarizabilities. In addition, when the laser wavelength is close to the $6s_{1/2} \to 6p_{1/2}$ transition, $\alpha_{6s} \to \infty$ for $\mathcal{A} = 0$ and $\mathcal{A} = -1$. However, for $\mathcal{A} = +1$, the polarizability of the $6s_{1/2,m=1/2}$ state remain finite. This is because the contributions of the scalar and vector terms from the $6s_{1/2} \to 6p_{1/2}$ transition cancel each other out, which is similar to Ca^+ ions.[45]

Figure 3 depicts the dynamic polarizabilities of the $6s_{1/2,m=1/2}$ and $5d_{3/2,m=3/2,1/2}$ states for the case of $\mathcal{A} = 0$. The crossings give rise to the magic wavelengths of the

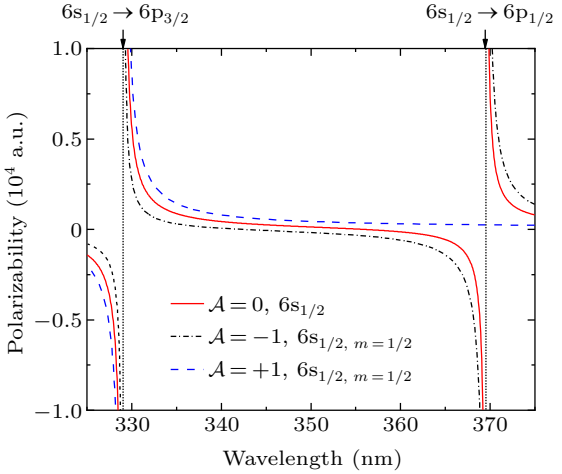


Fig. 2. Dynamic polarizabilities for the $6s_{1/2,m=1/2}$ state in the wavelength range 325 nm–375 nm in the $\mathcal{A} = 0$ and $\mathcal{A} = \pm 1$. The vertical dotted lines indicate the positions of the resonant $6s_{1/2} \to 6p_{1/2,3/2}$ transitions.

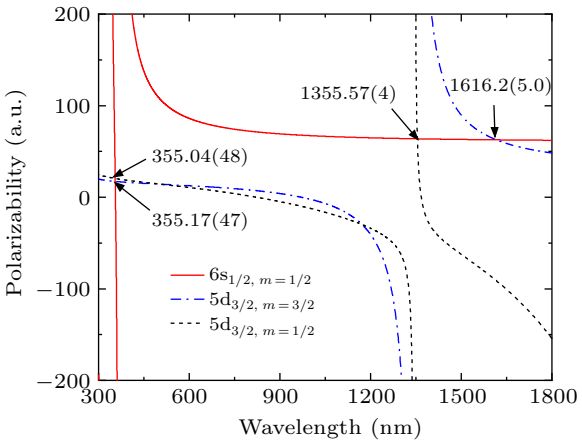


Fig. 3. Dynamic polarizabilities (in unit a.u.) of the $6s_{1/2,m=1/2}$ and $5d_{3/2,m=3/2,1/2}$ states in the case of $\mathcal{A} = 0$. The magic wavelengths are identified by arrows.

$6s_{1/2,m=1/2} \rightarrow 5d_{3/2,m=3/2,1/2}$ transitions and are identified by arrows. For each of the magnetic sublevel transitions, two magic wavelengths are found. One is near 355 nm, which lies between the resonant wavelengths of $6s_{1/2} \rightarrow 6p_{3/2}$ and $6s_{1/2} \rightarrow 6p_{1/2}$ transitions. Another one is larger than the resonant wavelength, 1345.63 nm, of $5d_{3/2} \rightarrow 6p_{3/2}$ transition.

Figure 4 presents the dynamic polarizabilities of the $6s_{1/2,m=1/2}$ and $5d_{3/2,m=\pm3/2,\pm1/2}$ states in the case of $\mathcal{A} = \pm1$. For each of magnetic sublevel transitions, two magic wavelengths are found in the case of $\mathcal{A} = -1$. One is near 340 nm, which lies between the resonant wavelengths of $6s_{1/2} \rightarrow 6p_{3/2}$ and $6s_{1/2} \rightarrow 6p_{1/2}$ transitions. The other one is larger than the resonant wavelength of $5d_{3/2} \rightarrow 6p_{3/2}$ transition, as shown in Figs. 4(a) and 4(c). In the case of $\mathcal{A} = +1$, only one magic wavelength of larger than the resonant wavelength of $5d_{3/2} \rightarrow 6p_{3/2}$ transition is found for each of magnetic sublevel transitions, as shown in Figs. 4(b) and 4(d).

Table 4 lists the differences between the magic wavelengths of $6s_{1/2,m=1/2} \rightarrow 5d_{3/2,m=\pm3/2,\pm1/2}$ transitions in the case of $\mathcal{A} = \pm1$ and $\mathcal{A} = 0$. The differences between the magic wavelengths which lies between the resonant wavelengths of $6s_{1/2} \rightarrow 6p_{3/2}$ and $6s_{1/2} \rightarrow 6p_{1/2}$ transitions of $\mathcal{A} = -1$ and $\mathcal{A} = 0$ are 12 nm–15 nm. This means that these magic wavelengths are sensitive to the degree of polarization of light. Moreover, the differences between the magic wavelengths which is larger than the resonant wavelength of $5d_{3/2} \rightarrow 6p_{3/2}$ transition of $\mathcal{A} = -1$ and $\mathcal{A} = 0$ are about 80 nm–270 nm, and the differences between magic wavelengths of $\mathcal{A} = +1$ and $\mathcal{A} = 0$ are about 85 nm–300 nm. These magic wavelengths are extremely sensitive to the degree of polarization of light.

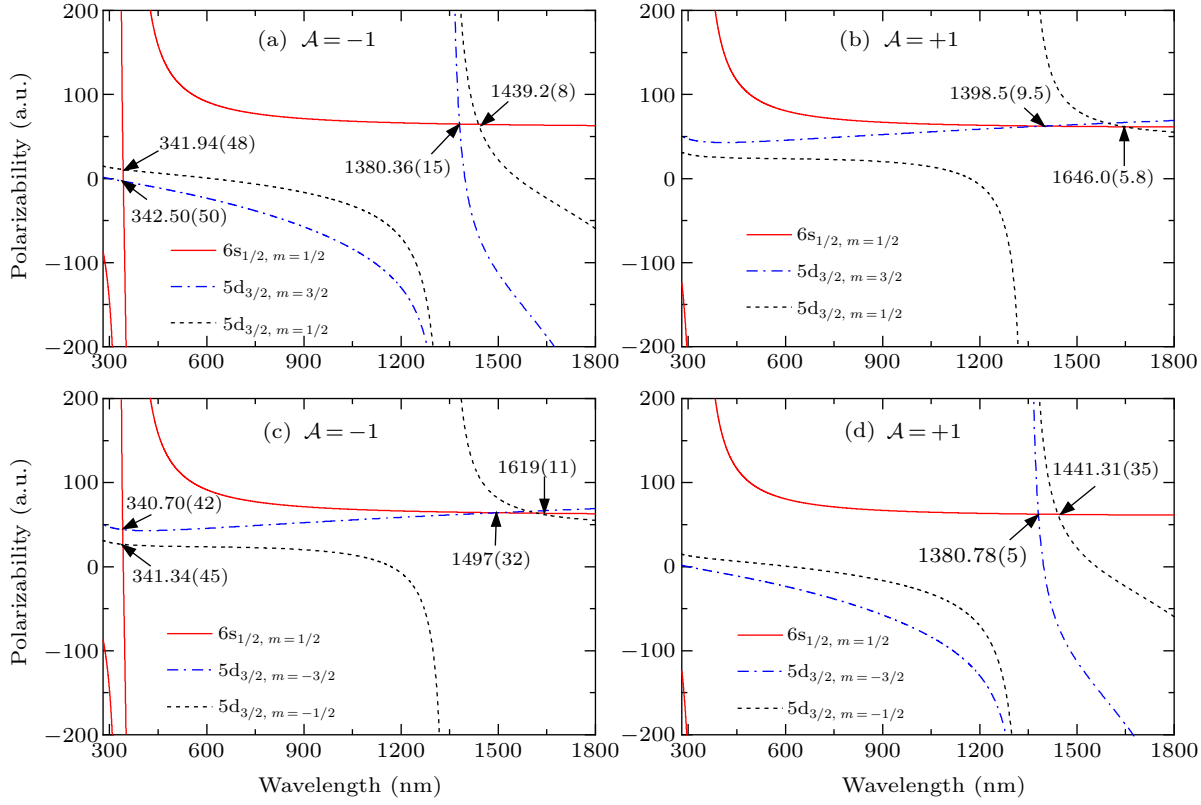


Fig. 4. Dynamic polarizabilities for the $6s_{1/2,m=1/2}$ and $5d_{3/2,m=\pm3/2,\pm1/2}$ states in the case of $\mathcal{A} = \pm1$. (a) and (b) The $6s_{1/2,m=1/2} \rightarrow 5d_{3/2,m=3/2,1/2}$ transitions in the case of $\mathcal{A} = \pm1$, respectively. (c) and (d) The $6s_{1/2,m=1/2} \rightarrow 5d_{3/2,m=-3/2,-1/2}$ transitions in the case of $\mathcal{A} = \pm1$, respectively. The obtained magic wavelengths are illustrated by arrows.

Table 4. Magic wavelengths (in unit nm) for the $6s_{1/2,m=1/2} \rightarrow 5d_{3/2,m=\pm3/2,\pm1/2}$ transitions in the case of $\mathcal{A} = \pm1$, which are compared with the ones in the case of $\mathcal{A} = 0$. $\Delta\lambda$ (in unit nm) denotes the difference of magic wavelengths between the case of $\mathcal{A} = \pm1$ and $\mathcal{A} = 0$.

$\mathcal{A} = 0$	$\mathcal{A} = -1$				$\mathcal{A} = +1$			
λ_{magic}	λ_{magic}	$\Delta\lambda$	λ_{magic}	$\Delta\lambda$	λ_{magic}	$\Delta\lambda$	λ_{magic}	$\Delta\lambda$
$6s_{1/2} \rightarrow 5d_{3/2,3/2}$	$6s_{1/2,1/2} \rightarrow 5d_{3/2,3/2}$		$6s_{1/2,1/2} \rightarrow 5d_{3/2,-3/2}$		$6s_{1/2,1/2} \rightarrow 5d_{3/2,3/2}$		$6s_{1/2,1/2} \rightarrow 5d_{3/2,-3/2}$	
1616.2(5.0)	1380.36(15)	−235.84	1497 (32)	−119.2	1398.5 (9.5)	−217.7	1380.78(5)	−235.42
355.17(47)	342.50(50)	−12.67	340.70(42)	−14.47				
$6s_{1/2} \rightarrow 5d_{3/2,1/2}$	$6s_{1/2,1/2} \rightarrow 5d_{3/2,1/2}$		$6s_{1/2,1/2} \rightarrow 5d_{3/2,-1/2}$		$6s_{1/2,1/2} \rightarrow 5d_{3/2,1/2}$		$6s_{1/2,1/2} \rightarrow 5d_{3/2,-1/2}$	
1355.57(4)	1439.2(8)	83.63	1619(17)	263.43	1646.0(5.8)	290.43	1441.31(35)	85.74
355.04(48)	341.94(48)	−13.10	341.34(45)	−13.70				

Figure 5 shows the dynamic polarizabilities of the $6s_{1/2}$ and $5d_{5/2,m=5/2,3/2,1/2}$ states in the case of $\mathcal{A}=0$. For each of magnetic sublevel transitions, only one magic wavelength is found, which is near 355 nm.

Figure 6 shows the dynamic polarizabilities of $6s_{1/2}$ and $5d_{5/2,m=\pm5/2,\pm3/2,\pm1/2}$ states in the case of $\mathcal{A}=\pm1$. In the case of $\mathcal{A}=-1$, only one magic wavelength is found for each transitions of $6s_{1/2,m=1/2} \rightarrow 5d_{5/2,m=5/2,\pm3/2,\pm1/2}$, which is near 340 nm. Two magic wavelengths are found for the $6s_{1/2,m=1/2} \rightarrow 5d_{5/2,m=-5/2}$ transition. However, in the case of $\mathcal{A}=+1$, one magic wavelength is found only for the $6s_{1/2} \rightarrow 5d_{5/2,m=5/2}$ transition, which is larger than 1200 nm. The differences between the magic wavelength of the $6s_{1/2,m=1/2} \rightarrow 5d_{5/2,m=\pm5/2,\pm3/2,\pm1/2}$ transitions in the case of $\mathcal{A}=\pm1$ and $\mathcal{A}=0$ are listed in Table 5. The differences between the magic wavelengths of $\mathcal{A}=-1$ and $\mathcal{A}=0$ are 12 nm–15 nm.

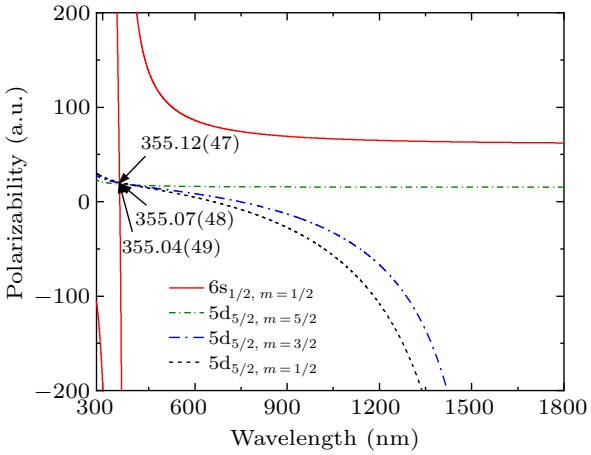


Fig. 5. The dynamic polarizabilities (in unit a.u.) of the $6s_{1/2}$ and $5d_{5/2,m=5/2,3/2,1/2}$ states in case of $\mathcal{A}=0$. The magic wavelengths are identified by arrows.

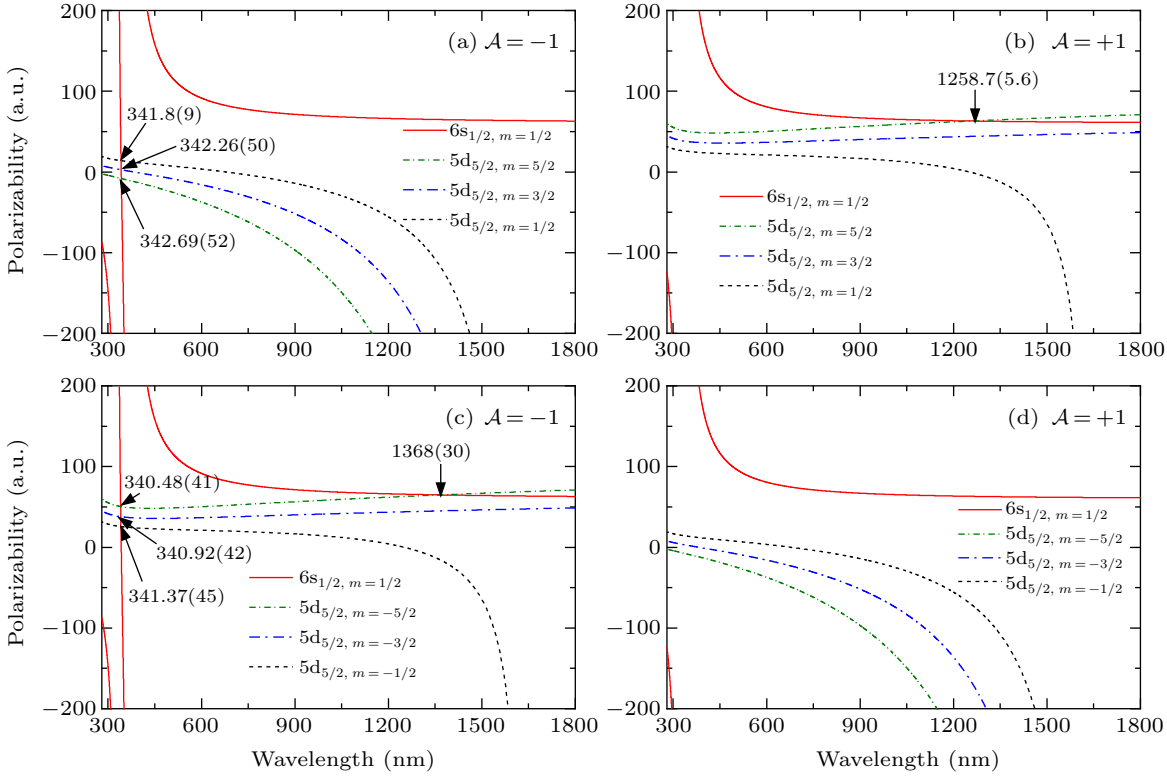


Fig. 6. Dynamic polarizabilities for the $6s_{1/2,m=1/2}$ and $5d_{5/2,m=\pm5/2,\pm3/2,\pm1/2}$ states in case of $\mathcal{A}=\pm1$. (a) and (b) The $6s_{1/2,m=1/2} \rightarrow 5d_{5/2,m=5/2,3/2,1/2}$ transitions in the case of $\mathcal{A}=\pm1$, respectively. (c) and (d) The $6s_{1/2,m=1/2} \rightarrow 5d_{5/2,m=-5/2,-3/2,-1/2}$ transitions in the case of $\mathcal{A}=\pm1$, respectively. The obtained magic wavelengths are illustrated by arrows.

Table 5. Magic wavelengths (in unit nm) for the $6s_{1/2,m=1/2} \rightarrow 5d_{5/2,m=\pm5/2,\pm3/2,\pm1/2}$ transitions for $\mathcal{A}=\pm1$, which are compared with the ones for $\mathcal{A}=0$. $\Delta\lambda$ (in unit nm) denotes the difference of magic wavelengths between the case of $\mathcal{A}=\pm1$ and $\mathcal{A}=0$.

$\mathcal{A}=0$	$\mathcal{A}=-1$				$\mathcal{A}=+1$			
λ_{magic}	λ_{magic}	$\Delta\lambda$	λ_{magic}	$\Delta\lambda$	λ_{magic}	$\Delta\lambda$	λ_{magic}	$\Delta\lambda$
$6s_{1/2} \rightarrow 5d_{5/2,5/2}$	$6s_{1/2,1/2} \rightarrow 5d_{5/2,5/2}$		$6s_{1/2,1/2} \rightarrow 5d_{5/2,-5/2}$		$6s_{1/2,1/2} \rightarrow 5d_{5/2,5/2}$		$6s_{1/2,1/2} \rightarrow 5d_{5/2,-5/2}$	
			1368(30)		1258.7(5.6)			
355.12(47)	342.69(52)	−12.43	340.48(41)	−14.64				
$6s_{1/2} \rightarrow 5d_{5/2,3/2}$	$6s_{1/2,1/2} \rightarrow 5d_{5/2,3/2}$		$6s_{1/2,1/2} \rightarrow 5d_{5/2,-3/2}$		$6s_{1/2,1/2} \rightarrow 5d_{5/2,3/2}$		$6s_{1/2,1/2} \rightarrow 5d_{5/2,-3/2}$	
355.07(48)	342.26(50)	−12.81	340.92(42)	−14.15				
$6s_{1/2} \rightarrow 5d_{5/2,1/2}$	$6s_{1/2,1/2} \rightarrow 5d_{5/2,1/2}$		$6s_{1/2,1/2} \rightarrow 5d_{5/2,-1/2}$		$6s_{1/2,1/2} \rightarrow 5d_{5/2,1/2}$		$6s_{1/2,1/2} \rightarrow 5d_{5/2,-1/2}$	
355.04(49)	341.8(9)	−13.24	341.37(45)	−13.67				

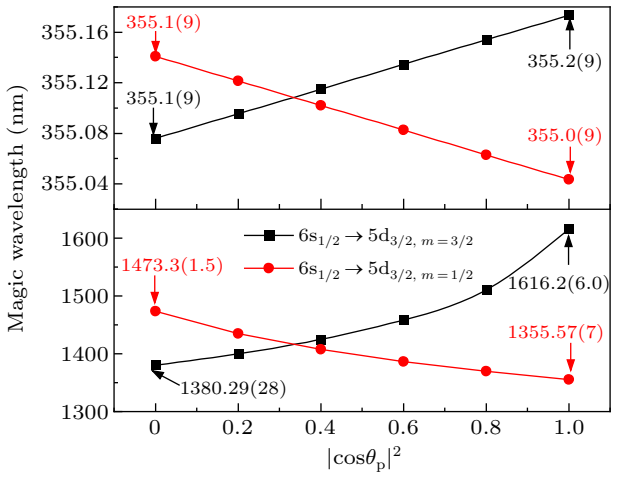


Fig. 7. The dependence of magic wavelengths of $6s_{1/2} \rightarrow 5d_{3/2,m=3/2,1/2}$ transitions upon $\cos^2\theta_p$ in the case of $\mathcal{A} = 0$.

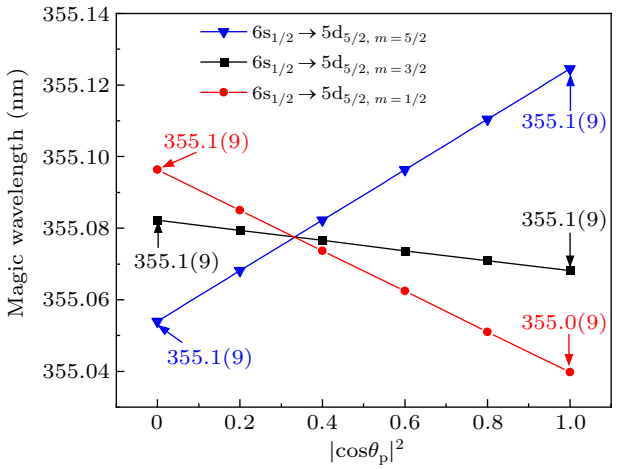


Fig. 8. The dependence of the magic wavelengths of $6s_{1/2} \rightarrow 5d_{5/2,m=5/2,3/2,1/2}$ transitions upon $\cos^2\theta_p$ in the case of $\mathcal{A} = 0$.

We have discussed the case of the direction of magnetic field $\hat{e}_z$ is parallel to the wave vector $\hat{k}$ in the above sections. However, when the direction of magnetic field is perpendicular to the wave vector, *i.e.*, $\cos\theta_k = 0$, the dynamic polarizability can be simplified as follows:

$$\alpha_i(\omega) = \alpha_i^{\mathrm{S}}(\omega) + \frac{3\cos^2\theta_p - 1}{2}\frac{3m^2 - j(j+1)}{j(2j-1)}\alpha_i^{\mathrm{T}}(\omega). \quad (12)$$

The θ_p is the angle between the $\hat{e}_z$ axis and direction of laser polarization $\hat{\varepsilon}$. The dynamic polarizability depends on not only the value of m but also the θ_p in a certain frequency ω.

Figure 7 shows the variation of the magic wavelengths for the $6s_{1/2} \rightarrow 5d_{3/2,m=3/2,1/2}$ transitions with $\cos^2\theta_p$. The upper panel shows the dependence of the magic wavelengths near 355 nm upon $\cos^2\theta_p$. As can be seen clearly, the magic wavelengths change nearly linearly with $\cos^2\theta_p$, and the magic wavelengths of each magnetic transition varies slowly with the increase of $\cos^2\theta_p$. The differences of magic wavelengths are less than 0.1 nm for the cases of $\cos^2\theta_p = 0$ and $\cos^2\theta_p = 1$. It means that these magic wavelengths are insensitive to the $\cos^2\theta_p$. The lower panel shows the $\cos^2\theta_p$ dependence of the magic wavelengths of larger than 1300 nm. The magic wavelength for the $6s_{1/2} \rightarrow 5d_{3/2,m=3/2}$ transition becomes longer with the increase of $\cos^2\theta_p$, while the magic wavelength for the $6s_{1/2} \rightarrow 5d_{3/2,m=1/2}$ transition becomes shorter. Moreover, these magic wavelengths vary sensitively with $\cos^2\theta_p$, and the differences are larger than 100 nm for the cases of $\cos^2\theta_p = 0$ and $\cos^2\theta_p = 1$.

Figure 8 shows the dependence of the magic wavelengths for the $6s_{1/2} \rightarrow 5d_{5/2,m=5/2,3/2,1/2}$ transitions upon $\cos^2\theta_p$. Similarly, the magic wavelengths near 355 nm are insensitive to $\cos^2\theta_p$. In addition, the uncertainties of these magic wavelengths are estimated using the uncertainties of the transition matrix elements.

4. Conclusion

The energy levels and E1 matrix elements of Yb^+ ions are calculated using the RCICP method. The static and dynamic polarizability of ground and low level states are determined. The magic wavelengths of the $6s_{1/2,m=1/2} \rightarrow 5d_{3/2,m=\pm3/2,\pm1/2}$ and $6s_{1/2,m=1/2} \rightarrow 5d_{5/2,m=\pm5/2,\pm3/2,\pm1/2}$ transitions are also determined.

For each of the $6s_{1/2,m=1/2} \rightarrow 5d_{3/2,m=\pm3/2,\pm1/2}$ transitions, two magic wavelengths are found in the case of $\mathcal{A} = 0$ and $\mathcal{A} = -1$. One of them lies between the resonant wavelengths of $6s_{1/2} \rightarrow 6p_{3/2}$ and $6s_{1/2} \rightarrow 6p_{1/2}$ transitions. This magic wavelength is sensitive to the degree of polarization of light ($\mathcal{A}$), but not to the angle between the direction of the magnetic field ($\hat{e}_z$ axis) and direction of laser polarization. Another one is larger than 1300 nm, and this magic wavelength is extremely sensitive to the the degree of polarization of light and the angle between the direction of the magnetic field and the direction of laser polarization. In the case of $\mathcal{A} = +1$, only one magic wavelength of larger than 1300 nm is found for each of the magnetic sublevel transitions. This magic wavelength is sensitive to the degree of polarization of light as well.

For each of the $6s_{1/2,m=1/2} \rightarrow 5d_{5/2,m=5/2,\pm3/2,\pm1/2}$ transitions, only one magic wavelength is found in the case of $\mathcal{A} = 0$ and $\mathcal{A} = -1$, which lies between the resonant wavelengths of $6s_{1/2} \rightarrow 6p_{3/2}$ and $6s_{1/2} \rightarrow 6p_{1/2}$ transitions. Moreover, this magic wavelength is also sensitive to the degree of polarization of light, but not sensitive to the angle between the direction of the magnetic field and direction of laser polarization. In the case of $\mathcal{A} = +1$, one magic wavelength is found only for the $6s_{1/2,m=1/2} \rightarrow 5d_{5/2,m=5/2}$ transition, which is larger than 1200 nm.

Acknowledgments

Project supported by the National Key Research and Development Program of China (Grant No. 2022YFA1602500),

the National Natural Science Foundation of China (Grant Nos. 12174316 and 12174268), the Young Teachers Scientific Research Ability Promotion Plan of Northwest Normal University (Grant No. NWNU-LKQN2020-10), the Innovative Fundamental Research Group Project of Gansu Province, China (Grant No. 20JR5RA541), and the Project of the Educational Commission of Guangdong Province of China (Grant No. 2020KTSCX124).

References

[1] Katori H, Ido T and Gonokami M K 1999 *J. Phys. Soc. Jpn.* **68** 2479
[2] Ye J, Vernooy D W and Kimble H J 1999 *Phys. Rev. Lett.* **83** 4987
[3] Takamoto M and Katori H 2003 *Phys. Rev. Lett.* **91** 223001
[4] Quinn T 2005 *Metrologia* **42** E01
[5] Wu X M, Li C B, Tang Y B and Shi T Y 2016 *Chin. Phys. B* **25** 093101
[6] Angstmann E J, Dzuba V A and Flambaum V V 2006 *Phys. Rev. Lett.* **97** 040802
[7] Chou C W, Hume D B, Koelemeij J C, Wineland D J and Rosenband T 2010 *Phys. Rev. Lett.* **104** 070802
[8] Huntemann N, Sanner C, Lipphardt B, Tamm C and Peik E 2016 *Phys. Rev. Lett.* **116** 063001
[9] Huntemann N, Okhapkin M, Lipphardt B, Weyers S, Tamm C and Peik E 2012 *Phys. Rev. Lett.* **108** 090801
[10] Gill P, Barwood G P, Klein H A, Huang G, Webster S A, Blythe P J, Hosaka K, Lea S N and Margolis H S 2003 *IEEE Meas. Sci. Technol.* **14** 1174
[11] Peik E, Lipphardt B, Schnatz H, Schneider T, Tamm C and Karshenboim S G 2004 *Phys. Rev. Lett.* **93** 170801
[12] Tamm C, Weyers S, Lipphardt B and Peik E 2009 *Phys. Rev. A* **80** 043403
[13] Peik E, Schneider T and Tamm C 2006 *J. Phys. B* **39** 145
[14] Yu N and Maleki L 2000 *Phys. Rev. A* **61** 022507
[15] Taylor P, Roberts M, Gateva-Kostova S V, Clarke R B M, Barwood G P, Rowley W R C and Gill P 1997 *Phys. Rev. A* **56** 2699
[16] Tamm C, Lipphardt B, Schnatz H, Wynands R, Weyers S, Schneider T and Peik E 2007 *IEEE Trans. Instrum. Mes.* **56** 601
[17] Ding L Y, Zhang Q X, Zhu C C, Wang Y X, Zhang X and Zhang W 2021 *Sci. Sin.-Phys. Mech. Astron.* **51** 074206
[18] Sahoo B K and Das B P 2011 *Phys. Rev. A* **84** 010502
[19] Flambaum V V, Geddes A J and Viatkina A V 2018 *Phys. Rev. A* **97** 032510
[20] Counts I, Hur J, Diana P L, Aude C, Jeon H, Leung C, Berengut J C, Geddes A, Kawasaki A, Jhe W and Vuletic V 2020 *Phys. Rev. Lett.* **125** 123002
[21] Dzuba V A, Flambaum V V, Safronova M S, Porsev S G, Pruttivarasin T, Hohensee M A and Häffner H 2016 *Nat. Phys.* **12** 465
[22] Monroe C, Campbell W C, Duan L M, Gong Z X, Gorshkov A V, Hess P W, Islam R, Kim K, Linke N M, Pagano G, Richerme P, Senko C and Yao N Y 2021 *Rev. Mod. Phys.* **93** 025001
[23] Porsev S G, Safronova M S and Kozlov M G 2012 *Phys. Rev. A* **86** 022504
[24] Jiang J, Mitroy J, Cheng Y J and Bromley M W J 2016 *Phys. Rev. A* **94** 062514
[25] Grant I P 1989 *Relativistic, Quantum Electrodynamic and Weak Interaction Effects in Atoms* (New York: AIP) p. 235
[26] Grant I P 2007 *Relativistic Quantum Theory of Atoms and Molecules: Theory and Computation* (New York: Springer) p. 797
[27] Roy A, De S, Arora B and Sahoo B K 2017 *J. Phys. B* **50** 205201
[28] Kien L F, Schneeweiss P and Rauschenbeutel A 2013 *Eur. Phys. J. D* **67** 92
[29] Manakov N L, Ovsiannikov V D and Rapoport L P 1986 *Phys. Rep.* **141** 320
[30] Beloy K 2009 "Theory of the ac Stark Effect on the Atomic Hyperfine Structure and Applications to Microwave Atomic Clocks", Ph.D thesis (Reno: University of Nevada)
[31] Mitroy J, Griffin D C, Norcross D W and Pindzola M S 1988 *Phys. Rev. A* **38** 3339
[32] Marinescu M, Sadeghpour H R and Dalgarno A 1994 *Phys. Rev. A* **49** 5103
[33] Hafner P and Schwarz W H E 1978 *J. Phys. B* **11** 217
[34] Kolb D, Johnson W R and Shorer P 1982 *Phys. Rev. A* **26** 19
[35] Safronova U I and Safronova M S 2009 *Phys. Rev. A* **79** 022512
[36] Biémont E, Dutrieux J F, Martin I and Quinet P 1998 *J. Phys. B* **31** 3321
[37] Olmschenk S, Younge K C, Moehring D L, Matsukevich D N, Maunz P and Monroe C 2007 *Phys. Rev. A* **76** 052314
[38] Olmschenk S, Hayes D, Matsukevich D N, Maunz P, Moehring D L, Younge K C and Monroe C 2009 *Phys. Rev. A* **80** 022502
[39] Pinnington E H, Berends R W and Ji Q 1994 *Phys. Rev. A* **50** 2758
[40] Kramida A 2013 *Fusion. Sci. Technol.* **63** 313
[41] Jiang J, Li X J, Wang X, Dong C Z and Wu Z W 2020 *Phys. Rev. A* **102** 042823
[42] Migdalek J 1982 *J. Quantum Spectrosc. Radiat. Transfer* **28** 61
[43] Lea S N, Webster S A and Barwood G P 2006 *Proceedings of the 20th European Frequency and Time Forum (EFTF)*, March 27–30, PTB Braunschweig, Germany, p. 302
[44] Schnei K.der T, Peik E and Tamm C 2005 *Phys. Rev. Lett.* **94** 230801
[45] Jiang J, Jiang L, Wang X, Zhang D H, Xie L Y and Dong C Z 2017 *Phys. Rev. A* **96** 042503